Computational approach to determine the relative biological effectiveness of fast neutrons using the Geant4-DNA toolkit and a DNA atomic model from the Protein Data Bank

Azam Zabihi

Department of Physics, Faculty of Science, Bu-Ali Sina University, Hamedan 651744161, Iran

Sebastien Incerti

University of Bordeaux, CENBG, UMR No. 5797, 33170 Gradignan, France
CNRS, IN2P3, CENBG, UMR No. 5797, 33170 Gradignan, France

Ziad Francis

Department of Physics, Faculty of Sciences, Université Saint Joseph, 2020 1104 Beirut, Lebanon

Ghasem Forozani

Department of Physics, Payame Noor University, P.O. Box 19395-3697, Tehran, Iran

Farid Semsarha

Institute of Biochemistry and Biophysics, University of Tehran, P.O. Box 13145-1384, Tehran, Iran

Amir Moslehi and Peiman Rezaeian

Radiation Applications Research School, Nuclear Science and Technology Research Institute, P.O. Box 11365-3486, Tehran, Iran

Mario A. Bernal[*]

Instituto de Física Gleb Wataghin, Universidade Estadual de Campinas, Campinas, 13083-859 São Paulo, Brazil

This study proposes an innovative approach to estimate relative biological effectiveness (RBE) of fast neutrons using the Geant4 toolkit. The Geant4-DNA version cannot track heavy ions below 0.5 MeV/nucleon. In order to explore the impact of this issue, secondary particles are simulated instead of the primary low-energy neutrons. The Evaluated Nuclear Data File library is used to determine the cross sections for the elastic and inelastic interactions of neutrons with water and to find the contribution of each secondary particle spectrum. Two strategies are investigated in order to find the best possible approach and results. The first one takes into account only light particles, protons produced from elastic scattering, and α particles from inelastic scattering. Geantino particles are shot instead of heavy ions; hence all heavy ions are considered in the simulations, though their physical effects on DNA not. The second strategy takes into account all the heavy and light ions, although heavy ions cannot be tracked down to very low energies ($E < 0.5$ MeV/nucleon). Our model is based on the combination of an atomic resolution DNA geometrical model and a Monte Carlo simulation toolkit for tracking particles. The atomic coordinates of the DNA double helix are extracted from the Protein Data Bank. Since secondary particle spectra are used instead of simulating the interaction of neutrons explicitly, this method reduces the computation times dramatically. Double-strand break induction is used as the end point for the estimation of the RBE of fast neutrons. ^{60}Co γ rays are used as the reference radiation quality. Both strategies succeed in reproducing the behavior of the RBE$_{max}$ as a function of the incident neutron energy ranging from 0.1 to 14 MeV, including the position of its peak. A comparison of the behavior of the two strategies shows that for neutrons with energies less than 0.7 MeV, the effect of heavy ions would not be very significant, but above 0.7 MeV, heavy ions have an important role in neutron RBE.

I. INTRODUCTION

Nowadays, understanding of the mechanisms behind the effects induced by ionizing radiation in living beings remains a major challenge [1–4]. In this context, the DNA molecule is the main target in the cell and it has nanometric dimensions [5–7]. Simple and complex forms of damage have been observed and they are related to the micro- and nanoscale patterns of radiation action [8,9].

In recent decades, Monte Carlo track structure codes have become an important tool for modeling the interaction of ionizing particles with DNA and the subsequent damage. Monte Carlo track structure codes improve understanding of

---

[*]Corresponding author: mbernalrod@gmail.com

radiation track structure and its relation with DNA damage [10,11]. Geant4 (geometry and tracking) is an open source Monte Carlo (MC) toolkit, initially developed for high-energy particle simulations at CERN [1,12–14]. It has been extended to address the description of particle interactions with liquid water down to the eV energy scale with Geant4-DNA [1,13]. This extension has sparked the use of this code in microdosimetry and nanodosimetry applications, including computational radiobiology [10].

The structure of DNA has been known for over 60 years [15]. Modeling the DNA structure is the first step in studying how ionizing particles interact with this molecule. DNA geometrical models could be classified into three main types: linear segments or cylinders, simple volume models, and atomic-resolution models [16]. The DNA geometrical models can be combined with MC simulation of radiation transport in order to study the early DNA damage induced by ionizing particles. A biophysical model for linking the energy deposition process to the DNA damage also has been included in this approach.

Studies in this field have used different DNA geometrical models. Linear DNA segments without any internal geometry [17,18] and individual volumes representing sugar-phosphate groups and nitrogenous bases [19–22] have been used. The first atomistic DNA model was proposed by Pomplun [23], who used the coordinates of individual atoms of a short B-DNA segment for studying the damage yield due to the decay of ^{125}I. Each atom was represented by spheres with radius equal to that of the corresponding van der Waals radius. Moiseenko *et al.* [24] developed another atomistic model of the B-DNA and reported single- and double-strand breaks for 660-keV photon radiation. Coordinates of atoms constituting DNA and van der Waals radii were used. The atomic coordinates of the DNA double helix in the interphase were used by Friedland *et al.* [25] for building a model of the whole genome of a mammalian cell nucleus, including six DNA organization levels. Two van der Waals radii were used to represent each atom. Bernal *et al.* [26] developed an atomistic B-DNA model that accounts for five organization levels of the DNA. This study implements the Protein Data Bank (PDB) as the geometry with an atomic level description of the DNA molecule [27].

Reactor workers, airline crew members, and astronauts in long-term space missions receive significant neutron doses [28]. In comparison with x rays or γ rays with similar energy, neutrons deposit more energy along their path, thus causing more damage to the cells. Neutrons have null net charge, so they do not interact electromagnetically with an atom's electrons. Instead, they interact with atomic nuclei and produce secondary heavy particles through both elastic and inelastic collisions [29]. These secondary particles are responsible for the high relative biological effectiveness (RBE) of neutrons. For this reason, the use of fast neutron beams for cancer radiation therapy has been explored [30]. Fast neutron radiation therapy is a valuable method to treat radioresistant tumors with a high linear energy transfer radiation [31–33].

The relative biological effectiveness of neutrons depends on their energy. Ottolenghi *et al.* [34], Baiocco *et al.* [35], and Stewart *et al.* [36] recently reported neutron biological effectiveness for a wide range of initial energy states. The Geant4 Monte Carlo code [1,12–14], including its low-energy
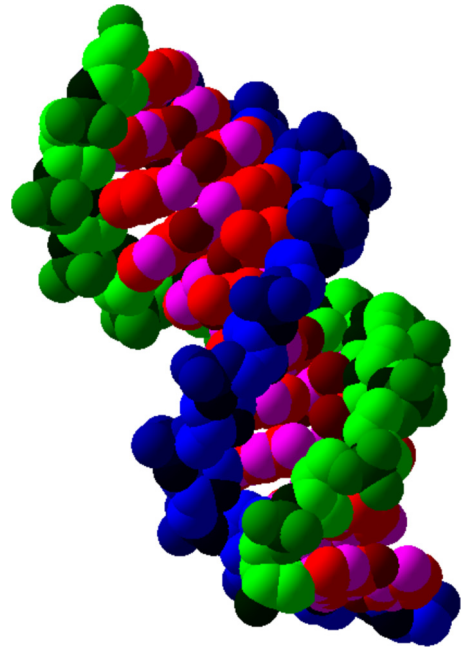

FIG. 1. The 1BNA structure from PDB shades of red are base atoms and shades of green and blue are the first- and second-strand atoms, respectively.

extension known as Geant4-DNA [1], is used to simulate the interaction of neutrons with liquid water. In Geant4-DNA there is however a limitation to tracking heavy ions below 0.5 MeV/nucleon. In order to explore the impact of this limitation, two strategies are proposed in this work. To save computation time, the interaction of neutrons with water is not explicitly simulated. Instead, secondary particles are sampled from the corresponding spectra. The Evaluated Nuclear Data File (ENDF) library is used to determine the angular differential cross section for elastic and inelastic interactions of neutrons with water and to find the contribution of each secondary particle spectrum. Performing neutron track structure simulations in relatively large volumes can be time consuming; therefore this approach also reduces computation times dramatically. Corresponding cross sections were used for sampling the emission of secondary heavy charged particles produced due to the impact of neutrons on water. The corresponding spectra were used to irradiate a PDB DNA atomic model and DSB yields were determined. These yields were used for estimating the neutrons RBE with different energies. ^{60}Co radiation was used as the reference radiation quality. The results of this work are compared with several other experimental and simulation-based values found in the literature.

II. METHODS

A. Biological target

An atomic resolution model of B-DNA was used in this study. B-DNA is the most probable structure of DNA in living cells [37]. The position of each atom in a double-helix segment was extracted from the PDB [38], specifically the 1BNA structure (Fig. 1) [39]. Atoms were modeled as

TABLE I. Relative contributions of different neutron interactions with water used in this work. These data were extracted from the ENDF database.

Energy (MeV)	H-elastic total (%)	O-elastic total (%)	O-inelastic total (%)
0.1	87.49	12.51	0.00
0.2	83.66	16.34	0.00
0.3	82.07	17.93	0.00
0.36	78.36	21.64	0.00
0.5	72.99	27.01	0.00
0.7	78.35	21.65	0.00
1	51.04	48.96	0.00
2	78.63	21.37	0.00
5	76.02	21.02	2.96
7	72.76	22.08	5.16
10	58.72	23.23	18.05
12	49.07	32.03	18.90
14	46.32	32.26	21.42

spheres with dimensions according to the corresponding van der Waals radius [27]. The PDB structure enables the use of an atomic level description of the DNA molecule. The cell nucleus contains 6×10^9 base pairs (bp), with 1BNA fragments uniformly distributed into a sphere with radius of 2.93 μm [40]. This nucleus will be referred to as the region of interest (ROI). The whole ROI was filled with 1.0 g cm^{-3} density water.

B. Irradiation setup

The current Geant4-DNA package has a limitation to tracking heavy ions below 0.5 MeV/nucleon. In order to overcome this restriction, a theoretical calculation and an MC computational approach are presented to model the effect of the tracking of heavy ions below 0.5 MeV/nucleon. Neutrons can interact with nuclei by several mechanisms. The secondary charged particles produced by fast neutrons with energy ranging from 0.1 to 14 MeV are studied in this work. Instead of directly emitting monoenergetic neutrons onto the ROI, the initial energy of secondary charged particles is sampled from the corresponding spectra. The initial position is uniformly distributed through the ROI and the corresponding direction is sampled isotropically. The secondary charged particles produced by fast neutrons transfer their energy to the medium mainly by ionization and excitation. In this way, the simulation time is reduced.

The ENDF/B-VI [41] is used to determine cross sections and angular differential cross sections of secondary particles, for elastic and inelastic interactions of neutrons with water, which contains hydrogen and oxygen. Elastic scattering is the only important process for the neutron-hydrogen interaction in the energy range of this study, which produces secondary protons. For neutron-oxygen collisions, elastic scattering is dominant below 5 MeV. Above this energy, inelastic scattering has a significant role, as shown in Table I. The hydrogen inelastic scattering cross section is negligible along the whole energy range of this work. Oxygen inelastic scattering cross sections can be discarded only for energies below about 5
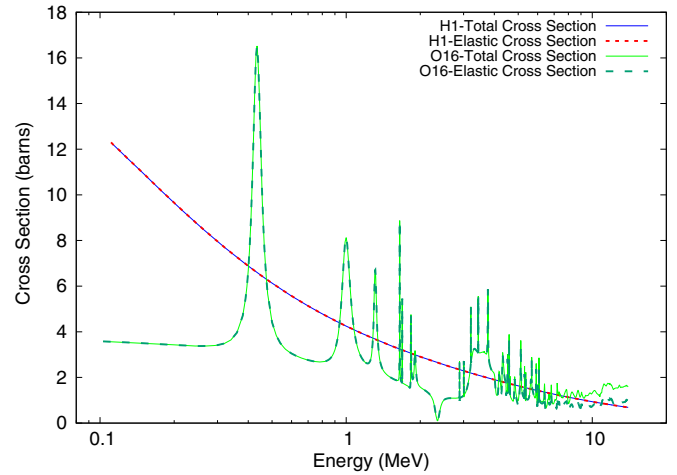

FIG. 2. Cross sections for the interaction of neutrons with water [41].

MeV. For higher energies, the contribution of the oxygen inelastic scattering cross section is dominant in the total cross section. The total cross section for neutron interaction with water can be approximated as [42]

$$\sigma_{\text{water}} = 2 \times \sigma_{\text{H}} + \sigma_{\text{O}}, \tag{1}$$

where σ_{H} and σ_{O} are the cross sections for the interaction with isolated H and O atoms, respectively. Another important point to mention is that the ^{16}O neutron cross sections have a resonance region in the energy range of the present work (Fig. 2). If a monoenergetic neutron beam coincides with one of the oxygen resonance peaks, the ratio of the cross section of oxygen to hydrogen can be as high as 2. The first peak is approximately at 0.47 MeV and after 1 MeV there are several peaks. In the present work and also others, monoenergetic neutrons are used. Because of the existence of the oxygen cross-section resonance, selecting the energy of the monoenergetic neutrons plays an important role. This means that the choice of neutron energy plays a significant role in the determination of the RBE and also in the comparison with previous results.

Table I presents the contribution from elastic and inelastic cross sections when neutrons impact on water atoms. These data were extracted from the ENDF database. For each neutron energy and scattering type, the initial energy of secondary particles was sampled using their corresponding spectra, which is explained below.

1. Elastic scattering

As mentioned above, the most important interaction mechanism for fast neutron energies below 5 MeV is elastic scattering. In the elastic collision between a neutron with energy T and a nucleus of mass number A, the maximum energy transferred to the recoiling nucleus is

$$\Delta T_{\max} = \frac{4A}{(1+A)^2} T. \tag{2}$$

A neutron gives up all its energy to hydrogen with $A = 1$ and gives up to 22.1% its energy to oxygen with $A = 16$. With the corresponding differential cross section of the recoiled

TABLE II. Contribution of oxygen inelastic cross sections to water total inelastic cross section (in %) (*n*, neutron; *a*, alpha; *p*, proton; and *D*, deuteron).

Reaction	Energy (MeV) 5	7	10	12	14
$^{16}O(n, a)\,^{13}C$	2.96	3.13	7.57	7.08	4.78
$^{16}O(n, n + a)\,^{12}C$	0.00	0.0	0.00	0.89	4.18
$^{16}O(n, D)\,^{15}N$	0.00	0.0	0.00	0.07	0.57
$^{16}O(n, p)\,^{16}N$	0.00	0.0	0.00	1.30	1.42
$^{16}O(n, n + p)\,^{15}N$	0.00	0.0	0.00	0.00	0.15
$^{16}O(n, 2n)\,^{15}O$	0.00	0.0	0.00	0.00	0.0

nucleus, the spectrum of scattered nuclei can be determined. The ENDF contains differential elastic cross sections in terms of the neutron scattering angle. Starting from the neutron scattering angle and using conservation laws, the nucleus emission angle can be determined, supposing that the latter is initially free and at rest. Using the chain derivation rule, neutron and recoiled nucleus differential scattering cross sections are correlated as

$$\frac{d\sigma}{d\Omega(\theta)} = \frac{d\sigma}{d\Omega(\phi)} \times \frac{d\Omega(\phi)}{d\Omega(\theta)}, \qquad (3)$$

where ϕ and θ are neutron and recoiled nucleus scattering angles, respectively. This is a standard prescription for relating angular distributions of two colliding particles. Accordingly, energy spectra of recoiled nuclei are obtained using Table 5 of Ref. [43]. Below 5 MeV, energy spectra of recoiled nuclei, protons, and oxygen are used as the initial energy of secondary particles.

2. Inelastic scattering

Above 5 MeV, the inelastic scattering of neutron with oxygen represents a significant contribution to the total interaction cross section. Inelastic interactions can lead to the fragmentation of the nucleus into two or more recoiled fragments. Generally, the lightest nuclei are used to represent the incident projectile and the emitted particle. The heaviest element in the exit channel is obtained by baryon number conservation. More details about inelastic scattering are shown in Table II. Like elastic scattering, by applying momentum and total energy conservation and adding the differential cross section for the inelastic interaction of neutrons with water, three equations with three unknown variables are found, which have a unique solution. Table II shows that the $^{16}O(n, \alpha)\,^{13}C$ reaction has the most contributions in inelastic scatterings. Accordingly, this study only considers the $^{16}O(n, \alpha)\,^{13}C$ reaction for inelastic scattering.

3. Definition of two strategies

As discussed above, heavy ions cannot be tracked down below 0.5 MeV/nucleon with the current Geant4-DNA version. Thus, heavy ions play a key role in simulation and obtaining results. In elastic scattering neutron energy is transferred to the proton and oxygen and in inelastic scattering, neutron energy is transferred to the light particle α and heavy ion ^{13}C. Two strategies are assumed to find the best possible approach

and results. The first one is shooting out only light particles, protons for elastic scattering and α particles for inelastic scattering. Geant4-DNA deals well with light particles down to very low energies in water, but this is not the case for heavy particles in the same energy range. Geantino[1] particles are shot instead of heavy ions in elastic and inelastic scattering. Hence heavy ions are accounted for, but their physical effects are not considered in the simulation. Thus, this procedure discards relatively-high-energy transfers caused by heavy ions.

The second strategy is shooting all light and heavy ions. Geant4-DNA cannot follow heavy ions with energy less than 0.5 MeV/nucleon. This means that heavy ions with energy less than 0.5 MeV/nucleon transfer all of their energy in a single collision. Hence their physical effects are considered in the simulation, yet in a limited way since there is not a suitable method to describe their energy depositions accurately.

C. Monte Carlo simulation

The recently released Geant4.10.2 [44] and the Geant4-DNA [1,12–14] extension were used for carrying out the simulations, including the interaction of ions and electrons with liquid water. Using Geant4-DNA with different physical models has shown that low-energy electron physics alone may strongly influence DNA damage yields [45]. This is a very important question since electrons are responsible for about 70% of the energy deposition events for primary heavy charged particles like protons and α particles [46]. Physical processes can generate detailed track structures of particles at the cellular and DNA scales. The default physics constructor, named G4EmDNAPhysics, was used. The energy cutoff for electrons is 7.4 and 100 eV for protons and 1 keV for α particles. As said before, this Geant4 version cannot follow heavy ions (carbon and heavier ions) below 0.5 MeV/nucleon.

D. Direct effects: Single- and double-strand-break damage

This work only accounts for direct damage. In this biophysical model, a single-strand break (SSB) occurs if any sugar-phosphate atom is hit with an energy deposit value greater than 10.79 eV, which is the first ionization level of liquid water [22,25]. A double-strand break (DSB) is accounted for if two SSBs are formed on opposite strands and separated by no more than 10 bp [22].

E. Calculation of RBE

This work estimates the RBE as the ratio between the DSB yield for the neutron beam in question and that determined for the reference quality, which is ^{60}Co [47]:

$$\mathrm{RBE_{DSB}} = \frac{Y_{\mathrm{DSB\ neutron}}}{Y_{\mathrm{DSB\ ^{60}Co}}}. \qquad (4)$$

It is also needed to calculate the DSB yield for ^{60}Co photons. An approach similar to that followed for neutrons is implemented for ^{60}Co. Secondary electrons produced by these photons are sampled and used to irradiate the ROI. This

---

[1] A Geantino is an artificial particle from Geant4 which is used as a geometrical probe and does not interact in the medium.

TABLE III. ^{60}Co SSB and DSB yields. Uncertainties represent one standard deviation of the mean. Here vdW denotes the number of van der Waals radii used for representing atoms.

Monte Carlo code	Source	Geometry	Size (vdW units)	SSB yield $(10^9$ Gy bp$)^{-1}$	DSB yield $(10^9$ Gy bp$)^{-1}$	SSB threshold energy (eV)
PARTRAC[a]	^{60}Co γ rays	atomic	2	92 ± 5	4.9 ± 0.1	10.79
Geant4-DNA[b]	secondary electrons from ^{60}Co γ rays	atomic	1	73.506 ± 0.006	3.80 ± 0.08	10.79

[a]Reference [25].
[b]Present study.

method has been tested and validated by Semsarha *et al.* [48] and Tajik *et al.* [49], which is much more efficient than starting from the corresponding photons.

III. RESULT AND DISCUSSION

A. Direct SSB and DSB yields of ^{60}Co

The SSB and DSB yields are shown in Table III and compared with those reported by Friedland *et al.* [25]. These results only account for the direct damage. The SSB yield values are 73.506 [$(10^9$ Gy bp$)^{-1}$] and 92 [$(10^9$ Gy bp$)^{-1}$] for this study and that of Friedland *et al.*, respectively. This yield depends on the energy threshold for an SSB induction and the sizes of the atoms conforming the sugar-phosphate group. This study uses the same threshold energy as Friedland *et al.* [25]. They used two van der Waals radii to represent the atoms, whereas one van der Waals radius is considered in this work. This may be the reason for the underestimation of SSB yield compared with those reported by Friedland *et al.* In our work, the Geant4-DNA toolkit is used for particle transport simulations, while Friedland *et al.* used their own code. The DSB yield obtained here is lower than that reported by Friedland *et al.* It should be remarked that we use the same definition of a DSB as them, so their higher DSB yield should be explained by their also higher SSB yield. In addition, the particularities of the MC code used could influence this yield, which depends on the clustering capacity of the energy

depositions. As stated before, the DSB yield for ^{60}Co photons will be used as reference for neutron RBE determination.

B. Fast neutron RBE

The fraction of the number of the produced secondary light and heavy charged particles obtained by the present work is shown in Table IV. The present data are also compared with Geant4 results that were obtained by explicitly simulating the direct shooting of neutrons into a sphere of 1.0 cm radius that was filled with 1.0 g cm^{-3} of water. The corresponding mean free path is approximately 0.99 cm. It is obvious from Table IV that both methods produce approximately similar values. Thus, this demonstrates that the approach used to obtain secondary particles has been validated.

According to Eq. (2), a neutron can transfer up to 22.1% of its energy to an oxygen atom during an elastic collision. Consequently, it is obvious that for neutron inelastic scattering with oxygen, energy transferred to carbon atoms is less than 22.1%. This leads to an absorbed dose into the ROI of about 0.11 and 15.4 Gy, respectively, for the first energy, 0.1 MeV, and the last neutron energy, 14 MeV. Hence a high-dose single event occurs for heavy ions at the end of their lives. Another point to consider is that the maximum transferred energy from a neutron to a proton, in a hydrogen atom, is nearly the whole energy of neutron. Also, as Table I shows for fast neutrons with $E < 10$ MeV, secondary protons produced by elastic interactions with hydrogen have a relatively high

TABLE IV. Fraction of the number of hydrogen and oxygen particles for elastic scattering and α particles for inelastic scattering produced by the impact of neutrons with water, compared with another Geant4 simulation [50].

Energy (MeV)	H-Geant4[a] (%)	H-ENDF (%)	O+α[a] (%)	O+α ENDF (%)
0.1	89.212	87.49	10.788	12.51
0.2	87.373	83.66	12.627	16.34
0.3	85.554	82.07	14.446	17.93
0.37	82.667	78.36	17.333	21.64
0.5	77.236	72.99	22.764	27.01
0.7	80.609	78.35	19.391	21.65
1	63.228	51.04	36.772	48.96
2	78.651	78.63	21.349	21.37
5	74.241	76.02	25.759	23.98
7	72.743	72.76	27.257	27.24
10	57.746	58.72	42.254	41.28
12	48.556	49.07	51.444	50.93
14	45.759	46.32	54.241	53.68

[a]Reference [50].
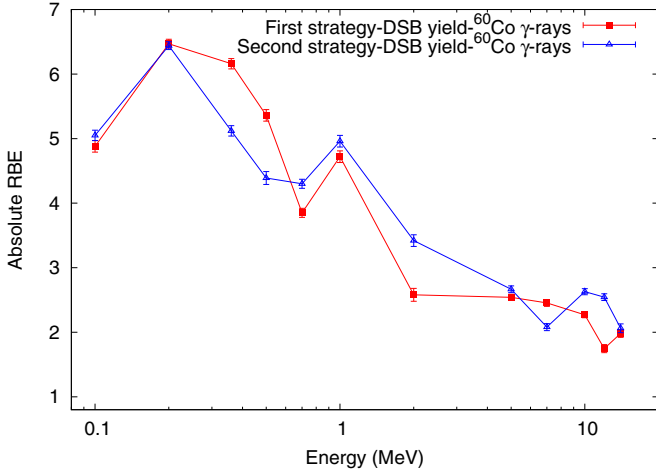
FIG. 3. Absolute RBE as a function of the incident neutron energy following both strategies.
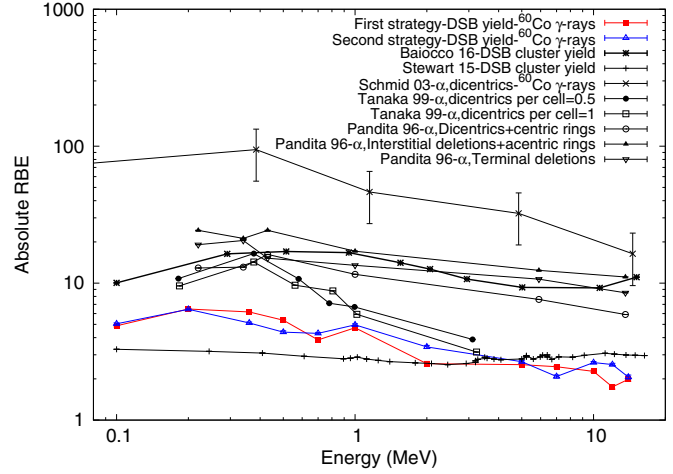

FIG. 4. Absolute RBE as a function of the incident neutron energy determined in this work using the DSB yield as the end point for first and second strategies. Corresponding values extracted from the other studies are also shown.

contribution that reaches almost more than twice that of heavy ions. In other words, below 10 MeV, light particles have a major role in neutron interactions with water. Here there is an exception: At 1 MeV, the contributions of light and heavy secondary particles are almost equal. Due to the high-dose single events of heavy ions and their low contribution to all secondary particles, two strategies were applied to specify the role of heavy particles in obtaining RBE. The RBE values as a function of incident neutron energy, for the first and second strategies, are compared in Fig. 3. The first strategy tracked down only protons and α particles and geantino particles were shot, instead of heavy ions. In the second strategy all secondary particles, light and heavy ions, were shot into the ROI. It can be observed in this figure that below 0.7 MeV, the RBE related to the first strategy is greater than those obtained through the second strategy, and after this point, this behavior is practically inverted. In addition, it is observed that secondary light particles have a dominant role in the RBE. As Eq. (2) and Table V show, the maximum energy transferred to heavy ions is less than that for light ions, 22.1% vs 100%. This fact, in conjunction with the less probable generation of heavy particles, means that heavy ions have a small contribution to the deposited energy and so to the DNA damage induction. Due to the Geant4-DNA limitation for tracking heavy ions, in the second strategy only one step is assumed for heavy ions with energy below 0.5 MeV/nucleon, during which they produce a very large energy deposition. If it occurs in sugar-

phosphate groups, it will be counted as only one strand break for a relatively high dose. Consequently, the second strategy tends to account for less damage per unit dose. Accordingly, the DSB yield for the second strategy tends to be lower than that for the first one.

Relative biological effectiveness values as a function of the incident neutron energy are compared with several experimental and numerical data in Fig. 4. The reference radiation quality used in this work is ^{60}Co γ rays. The experimental and numerical data mentioned used ^{60}Co γ rays, ^{137}Cs γ rays, or x rays as reference radiation qualities. The position of the RBE peak as a function of the neutron energy (RBE$_{max}$) should not depend on the biological end point or the reference radiation. The current results show an RBE$_{max}$ of 0.2 MeV, which agrees very well with the other results shown in Fig. 4. It is observed that, for all energies, the results for the first and second strategies show a trend similar to those of the other experimental and numerical data. Also, above 2 MeV, the RBE values from both strategies are closer to the data reported by Stewart *et al.* [36].

IV. CONCLUSION

In this work data extracted from the Protein Data Bank were used to model a DNA double-helix segment with atomic resolution. This model was combined with Geant4-based MC simulations to estimate the RBE of fast neutrons with energies ranging from 0.1 to 14 MeV. Below 2 MeV, elastic scattering is dominant for interactions of neutrons with hydrogen and oxygen atoms. For higher energies, the inelastic scattering contribution is important only for oxygen atoms. For energies below 0.5 MeV/nucleon, this Geant4-DNA version cannot follow ions heavier than α particles. To succeed in dealing with this issue, instead of neutrons, the secondary particles from the corresponding spectra were shot into nuclei. The secondary charged particle yields obtained by the present method were similar to those obtained by the explicit simulation of the neutron-water interaction, carried out with Geant4, which

TABLE V. Maximum energy transfer to oxygen for several neutron energies.

Incident neutron energy (MeV)	Maximum energy transferred (MeV)
0.1	0.022
0.2	0.044
0.36	0.079
12	2.652
14	3.094

validates our approach. The advantage of this procedure is to account for the contribution and the physical effects of heavy ions while reducing the computation time significantly. By applying two different strategies, this study presented an approach for exploring the impact of the transport of heavy ions with energies below 0.5 MeV/nucleon, which cannot be done with Geant4 yet. However, we are aware that a final conclusion may be found after the incorporation of this capacity into the Geant4 code. The inclusion of secondary heavy particles into the simulation influences damage yields in two ways: the possibility of induction of additional DNA breaks and the important increase of the energy (dose) deposited into the ROI. The interplay of these two factors may explain why the first strategy led to higher DSB yields for neutron energies below 0.7 MeV and the inverted behavior above this energy.

The existence of oxygen cross-section resonances made the selection of neutron energy very important during the determination of RBE. Therefore, comparing RBE obtained in different works is a very difficult task, without mentioning biological factors such as cell lines and assay methods. The RBE$_{max}$ values obtained by both strategies are consistent with those reported in the literature, mainly with similar works based on simulations. The position of the RBE peak as a function of the neutron energy obtained in this work is similar to those reported in simulated and experimental works.

[1] M. Bernal, M. Bordage, J. Brown, M. Davídková, E. Delage, Z. El Bitar, S. Enger, Z. Francis, S. Guatelli, V. Ivanchenko, *et al.*, Track structure modeling in liquid water: A review of the Geant4-DNA very low energy extension of the Geant4 Monte Carlo simulation toolkit, Phys. Med. **31**, 861 (2015).

[2] D. Viduna, K. Hinsen, and G. Kneller, Influence of molecular flexibility on DNA radiosensitivity: A simulation study, Phys. Rev. E **62**, 3986 (2000).

[3] M. B. Hahn, S. Meyer, H.-J. Kunte, T. Solomun, and H. Sturm, Measurements and simulations of microscopic damage to dna in water by 30 keV electrons: A general approach applicable to other radiation sources and biological targets, Phys. Rev. E **95**, 052419 (2017).

[4] E. Nováková, L. Vyšín, T. Burian, L. Juha, M. Davídková, V. Múčka, V. Čuba, M. E. Grisham, S. Heinbuch, and J. J. Rocca, Breaking DNA strands by extreme-ultraviolet laser pulses in vacuum, Phys. Rev. E **91**, 042718 (2015).

[5] M. Pinak and A. Ito, Energy deposition in structural parts of DNA by monoenergetic electrons, J. Radiat. Res. **34**, 221 (1993).

[6] M. Folkard, K. Prise, B. Vojnovic, S. Davies, M. Roper, and B. Michael, Measurement of DNA damage by electrons with energies between 25 and 4000 eV, Int. J. Radiat. Biol. **64**, 651 (1993).

[7] D. T. Goodhead, Initial events in the cellular effects of ionizing radiations: Clustered damage in DNA, Int. J. Radiat. Biol. **65**, 7 (1994).

[8] H. Nikjoo, S. Uehara, D. Emfietzoglou, and F. Cucinotta, Track-structure codes in radiation research, Radiat. Meas. **41**, 1052 (2006).

[9] H. Nikjoo, D. Emfietzoglou, R. Watanabe, and S. Uehara, Can Monte Carlo track structure codes reveal reaction mechanism in DNA damage and improve radiation therapy?, Radiat. Phys. Chem. **77**, 1270 (2008).

[10] S. Incerti, M. Douglass, S. Penfold, S. Guatelli, and E. Bezak, Review of Geant4-DNA applications for micro and nanoscale simulations, Phys. Med. **32**, 1187 (2016).

[11] H. Nikjoo, D. Emfietzoglou, T. Liamsuwan, R. Taleei, D. Liljequist, and S. Uehara, Radiation track, DNA damage and response—A review, Rep. Prog. Phys. **79**, 116601 (2016).

[12] S. Incerti, I. Kyriakou, M. Bernal, M. Bordage, Z. Francis, S. Guatelli, V. Ivanchenko, M. Karamitros, N. Lampe, S. B. Lee *et al.*, Geant4-DNA example applications for track structure simulations in liquid water: A report from the Geant4-DNA Project, Med. Phys. **45**, e722 (2018).

[13] S. Incerti, A. Ivanchenko, M. Karamitros, A. Mantero, P. Moretto, H. Tran, B. Mascialino, C. Champion, V. Ivanchenko, M. Bernal *et al.*, Comparison of Geant4 very low energy cross section models with experimental data in water, Med. Phys. **37**, 4692 (2010).

[14] S. Incerti, G. Baldacchino, M. Bernal, R. Capra, C. Champion, Z. Francis, P. Guèye, A. Mantero, B. Mascialino, P. Moretto *et al.*, The Geant4-DNA project, Int. J. Model. Simul. Sci. Comput. **1**, 157 (2010).

[15] J. D. Watson and F. H. C. Crick, Molecular structure of nucleic acids: A structure for deoxyribose nucleic acid, Nature **171**, 737 (1953).

[16] H. Nikjoo, P. O'Neill, M. Terrisol, and D. Goodhead, Quantitative modelling of DNA damage using Monte Carlo track structure method, Radiat. Environ. Biophys. **38**, 31 (1999).

[17] D. Charlton, The range of high LET effects from ^{125}I decays, Radiat. Res. **107**, 163 (1986).

[18] H. Nikjoo, D. Goodhead, D. Charlton, and H. Paretzke, Energy deposition in small cylindrical targets by monoenergetic electrons, Int. J. Radiat. Biol. **60**, 739 (1991).

[19] D. Charlton, H. Nikjoo, and J. Humm, Calculation of initial yields of single- and double-strand breaks in cell nuclei from electrons, protons and alpha particles, Int. J. Radiat. Biol. **56**, 1 (1989).

[20] F. Semsarha, B. Goliaei, G. Raisali, H. Khalafi, and L. Mirzakhanian, An investigation on the radiation sensitivity of dna conformations to ^{60}Co gamma rays by using Geant4 toolkit, Nucl. Instrum. Methods Phys. Res. Sect. B **323**, 75 (2014).

[21] G. Raisali, L. Mirzakhanian, S. F. Masoudi, and F. Semsarha, Calculation of DNA strand breaks due to direct and indirect effects of auger electrons from incorporated ^{123}I and ^{125}I radionuclides using the Geant4 computer code, Int. J. Radiat. Biol. **89**, 57 (2013).

[22] M. Bernal and J. Liendo, An investigation on the capabilities of the PENELOPE MC code in nanodosimetry, Med. Phys. **36**, 620 (2009).

[23] E. Pomplun, A new DNA target model for track structure calculations and its first application to I-125 auger electrons, Int. J. Radiat. Biol. **59**, 625 (1991).

[24] V. V. Moiseenko, R. N. Hamm, A. J. Waker, and W. V. Prestwich, The cellular environment in computer simulations of radiation-induced damage to DNA, Radiat. Environ. Biophys. **37**, 167 (1998).

[25] W. Friedland, P. Jacob, H. G. Paretzke, M. Merzagora, and A. Ottolenghi, Simulation of DNA fragment distributions after irradiation with photons, Radiat. Environ. Biophys. **38**, 39 (1999).

[26] M. A. Bernal, D. Sikansi, F. Cavalcante, S. Incerti, C. Champion, V. Ivanchenko, and Z. Francis, An atomistic geometrical model of the B-DNA configuration for DNA-radiation interaction simulations, Comput. Phys. Commun. **184**, 2840 (2013).

[27] E. Delage, Q. T. Pham, M. Karamitros, H. Payno, V. Stepan, S. Incerti, L. Maigne, and Y. Perrot, PDB4DNA: Implementation of DNA geometry from the Protein Data Bank (PDB) description for Geant4-DNA Monte-Carlo simulations, Comput. Phys. Commun. **192**, 282 (2015).

[28] R. C. Miller, S. A. Marino, S. G. Martln, K. Komatsu, C. R. Geard, D. J. Brenner, and E. J. Hall, Neutron-energy-dependent cell survival and oncogenic transformation, J. Radiat. Res. **40**, S53 (1999).

[29] R. L. Morgan, in *CYCLOTRONS—1972: Proceedings of the Sixth International Cyclotron Conference, Vancouver, 1972*, edited by H. C. Wolfe, J. J. Burgerjon, and A. Strathdee, AIP Conf. Proc. No. 9 (AIP, New York, 1972), pp. 562–577.

[30] R. S. Stone, J. H. Lawrence, and P. C. Aebersold, A preliminary report on the use of fast neutrons in the treatment of malignant disease, Radiology **35**, 322 (1940).

[31] M.-A. Timoshchuk, P. Dekker, D. S. Hippe, U. Parvathaneni, J. J. Liao, G. E. Laramore, and J. K. Dillon, The efficacy of neutron radiation therapy in treating salivary gland malignancies, Oral Oncol. **88**, 51 (2019).

[32] S. K. Schaub, R. D. Stewart, G. A. Sandison, T. Arbuckle, J. J. Liao, G. E. Laramore, J. Zeng, R. Rengan, Y. D. Tseng, N. A. Mayr *et al.*, Does neutron radiation therapy potentiate an immune response to Merkel cell carcinoma?, Int. J. Particle Therapy **5**, 183 (2018).

[33] T. Imaoka, M. Nishimura, K. Daino, A. Hosoki, M. Takabatake, T. Kokubo, K. Doi, K. Showler, Y. Nishimura, H. Moriyama *et al.*, Age modifies the effect of 2-MeV fast neutrons on rat mammary carcinogenesis, Radiat. Res. **188**, 419 (2017).

[34] A. Ottolenghi, G. Baiocco, V. Smyth, and K. Trott, The ANDANTE project: A multidisciplinary approach to neutron RBE, Radiat. Prot. Dosim. **166**, 311 (2015).

[35] G. Baiocco, S. Barbieri, G. Babini, J. Morini, D. Alloni, W. Friedland, P. Kundrát, E. Schmitt, M. Puchalska, L. Sihver *et al.*, The origin of neutron biological effectiveness as a function of energy, Sci. Rep. **6**, 34033 (2016).

[36] R. D. Stewart, S. W. Streitmatter, D. C. Argento, C. Kirkby, J. T. Goorley, G. Moffitt, T. Jevremovic, and G. A. Sandison, Rapid

[37] MCNP simulation of DNA double strand break (DSB) relative biological effectiveness (RBE) for photons, neutrons, and light ions, Phys. Med. Biol. **60**, 8249 (2015).

[37] A. Leslie, S. Arnott, R. Chandrasekaran, and R. Ratliff, Polymorphism of DNA double helices, J. Mol. Biol. **143**, 49 (1980).

[38] http://rcsb.org.

[39] H. R. Drew, R. M. Wing, T. Takano, C. Broka, S. Tanaka, K. Itakura, and R. E. Dickerson, Structure of a B-DNA dodecamer: Conformation and dynamics, Proc. Natl. Acad. Sci. USA **78**, 2179 (1981).

[40] B. Alberts, D. Bray, J. Lewis, M. Raff, K. Roberts, and J. D. Watson, Molecular Biology of the Cell, 3rd ed. (Garland, New York, 1994), Vol. 43, p. 67.

[41] Evaluated Nuclear Data File, Database version of 2017-03-10 and JEFF-3.2 (IAEA, Vienna).

[42] Y. Abe, T. Tsuboi, and S. Tasaki, Evaluation of the neutron scattering cross-section for light water by molecular dynamics, Nucl. Instrum. Methods Phys. Res. Sect. A **735**, 568 (2014).

[43] J. B. Marion, F. C. Young, and D. Bromley, Nuclear reaction analyses-graphs and tables, Am. J. Phys. **37**, 1070 (1969).

[44] J. Allison, K. Amako, J. Apostolakis, P. Arce, M. Asai, T. Aso, E. Bagli, A. Bagulya, S. Banerjee, G. Barrand *et al.*, Recent developments in Geant4, Nucl. Instrum. Methods Phys. Res. Sect. A **835**, 186 (2016).

[45] N. Lampe, M. Karamitros, V. Breton, J. M. Brown, I. Kyriakou, D. Sakata, D. Sarramia, and S. Incerti, Mechanistic DNA damage simulations in Geant4-DNA part 1: A parameter study in a simplified geometry, Phys. Med. **48**, 135 (2018).

[46] M. A. Bernal, C. E. deAlmeida, S. Incerti, C. Champion, V. Ivanchenko, and Z. Francis, The influence of DNA configuration on the direct strand break yield, Comput. Math. Method Med. **2015**, 417501 (2015).

[47] P. Pater, G. Bäckström, F. Villegas, A. Ahnesjö, S. A. Enger, J. Seuntjens, and I. El Naqa, Proton and light ion RBE for the induction of direct DNA double strand breaks, Med. Phys. **43**, 2131 (2016).

[48] F. Semsarha, G. Raisali, B. Goliaei, and H. Khalafi, Microdosimetry of DNA conformations: Relation between direct effect of ^{60}Co gamma rays and topology of DNA geometrical models in the calculation of A-, B-and Z-DNA radiation-induced damage yields, Radiat. Environ. Biophys. **55**, 243 (2016).

[49] M. Tajik, A. S. Rozatian, and F. Semsarha, Calculation of direct effects of ^{60}Co gamma rays on the different DNA structural levels: A simulation study using the Geant4-DNA toolkit, Nucl. Instrum. Methods Phys. Res. Sect. B **346**, 53 (2015).

[50] A. Zabihi, J. Tello, S. Incerti, Z. Francis, G. Forozani, F. Semsarha, A. Moslehi, and M. A. Bernal, Determination of fast neutron RBE using a fully mechanistic computational model (unpublished).